Long-range micro-pulse aerosol lidar at 1.5 μm with an upconversion single-photon detector

Haiyun Xia,[1,3] Guoliang Shentu,[2,4] Mingjia Shangguan,[1] Xiuxiu Xia,[2,4] Xiaodong Jia,[1] Chong Wang,[1] Jun Zhang,[2,4] Jason S. Pelc,[5] M. M. Fejer,[5] Qiang Zhang,[2,4,6] Xiankang Dou,[1,4,7] and Jian-Wei Pan[2,4,8]

[1]*CAS Key Laboratory of Geospace Environment, University of Science and Technology of China, Hefei 230026, China*

[2]*Shanghai Branch, National Laboratory for Physical Sciences at Microscale and Department of Modern Physics, University of Science and Technology of China, Shanghai 201315, China*

[3]*Collaborative Innovation Center of Astronautical Science and Technology, HIT, Harbin 150001, China*

[4]*Synergetic Innovation Center of Quantum Information and Quantum Physics, USTC, Hefei 230026, China*

[5]*Edward L. Ginzton Laboratory, Stanford University, Stanford, California 94305, USA*

[6]*e-mail: qiangzh@ustc.edu.cn*

[7]*e-mail: dou@ustc.edu.cn*

[8]*e-mail: pan@ustc.edu.cn*

Received December 9, 2014; revised February 12, 2015; accepted February 12, 2015; posted March 6, 2015 (Doc. ID 229306); published March 30, 2015

A micro-pulse lidar at eye-safe wavelength is constructed based on an upconversion single-photon detector. The ultralow-noise detector enables using integration technique to improve the signal-to-noise ratio of the atmospheric backscattering even at daytime. With pulse energy of 110 μJ, pulse repetition rate of 15 kHz, optical antenna diameter of 100 mm and integration time of 5 min, a horizontal detection range of 7 km is realized. In the demonstration experiment, atmospheric visibility over 24 h is monitored continuously, with results in accordance with the weather forecasts.

OCIS codes: (010.3640) Lidar; (010.0280) Remote sensing and sensors; (280.1100) Aerosol detection; (190.7220) Upconversion.

http://dx.doi.org/10.1364/OL.40.001579

As a minor constituent of the atmosphere, aerosols not only play an important role in the radiation budget, air chemistry, and hydrological cycle, but also affect the environment quality and the public health. The occurrence, residence time, physical properties, and chemical composition verifies fast in space and time due to variable aerosol sources and meteorological processes. Lidar is recognized as the only method that can provide global height-resolved observation of the aerosols [1].

For full-time automatic operation of lidars in the field, the issue of eye safety should be considered. Fortunately, the 1.5-μm laser shows the highest maximum permissible exposure in the wavelength ranging from 0.3 to 10 μm [2]. What is more, in contrast with UV and Visible systems, 1.5-μm lidars suffer lower atmospheric attenuation, minor disturbance from Rayleigh scattering, and weaker sky radiance.

During clear weather conditions, the pulse energy of the aerosol should be higher than 100 mJ to guarantee a detection range about 10 km [3]. However, the peak power of such a laser pulse is far beyond the stimulated brilliouin scattering (SBS) threshold of any erbium-doped fiber amplifier (EDFA) [4]. Thus, complex and expensive solid-state techniques including stimulated Raman scattering (SRS) [5], optical parametric oscillator [6], and resonator with Cr^{4+}: YAG crystal [7] are developed to generate high-power lasers at 1.5 μm for aerosol lidars.

In principle, the SNR of a lidar is dominated by the product of laser power and the telescope area. Although the detector used in a lidar finally decides the quality of the raw data, its contribution is often neglected. Because the quantum efficiency is usually treated as a constant, the cathode material of a detector is selected according to its sensitivity versus the working wavelength. For example, InGaAs avalanche photodiode (APD) is used for 1.5-μm detection commonly. But it suffers from low efficiency (about 18%), high noise (a few kHz) due to impurities, and defects of the cathode material [8–10]. Superconducting single-photon detector (SSPD) at optical communication band has the advantages of high efficiency (>90%), ultralow noise (<1 Hz), and low timing jitter (<100 ps) [11]. However, the requirement for liquid helium refrigeration equipment restricts their practical applications in many fields.

Generally, traditional micro-pulse lidar is thought quite unsuitable for long-range aerosol detection with high temporal/spatial resolution [3]. In this work, a compact micro-pulse aerosol lidar incorporating a fiber laser at 1.5 μm, a small optical antenna, and an upconversion detector (UCD) is proposed for long-range aerosol detection during day and night, as shown in Fig. 1.

The UCD upconverts photons at communication band to visible photons when quasi-phase matching (QPM) is achieved in a periodically poled lithium niobate waveguide (PPLN-W). Then single photons at 1.5 μm can be counted by using a Si: APD with high efficiency, low noise, and less afterpulsing [12].

At present, commercially available fiber lasers benefit from the reliable optic components widely used in the telecommunications industry. Here, the continuous wave from a seed laser (Keyopsys, PEFL-EOLA) is chopped into pulse train after passing through an acousto-optic modulator (AOM) (Gooch & Housego, T-M080). The AOM is driven by an arbitrary waveform generator (Agilent, 33250A), which determines the shape of the laser pulse and its repetition rate. The weak laser pulse is fed to a polarization-maintaining EDFA (Keyopsys, PEFA-EOLA), which delivers pulse train with pulse energy up to 110 μJ.

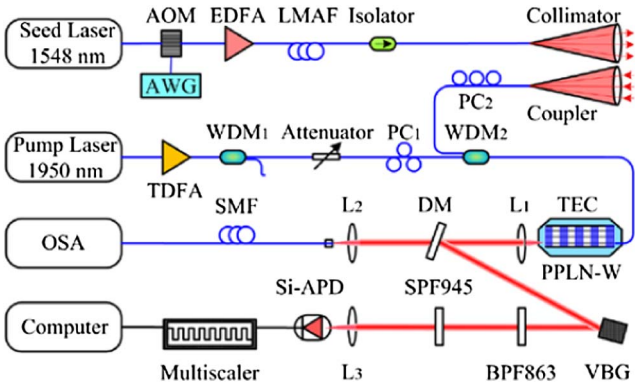

Fig. 1. System layout of the infrared aerosol lidar. AOM, acousto-optic modulator; AWG, arbitrary waveform generator; TDFA, thulium-doped fiber amplifier; LMAF, large-mode-area fiber; SMF, single-mode fiber; WDM, wavelength division multiplexer; PC, polarization controller; OSA, optical spectrum analyzer; DM, dichroic mirror; L, lens; SPF, short-pass filter; BPS, band-pass filter; VBG, volume Bragg grating; TEC, thermoelectric cooler.

A large mode area fiber with numerical aperture of 0.08 is used to increase the threshold of SBS and avoid self-saturation of amplified spontaneous emission (ASE). Then, the laser is collimated and sent to the atmosphere. It is worth a mention that the maximum permissible ocular exposure to the output laser beam is 255 mJ [2], which is far beyond the pulse energy of 110 μJ used here.

The backscattering from the atmosphere is coupled into a single-mode fiber by using a pigtail coupler. It should be noted that the micro-pulse transmitter at 1.5 μm with such a small optical antenna is generally used for object ranging with time-correlated single-photon counting technique [13] or atmosphere wind detection using heterodyne technique [14]. Direct detection of the weak aerosol backscattering signal is a great challenge for micro-pulse lidars. Similar to previous works [15–18], an upconversion single-photon detector is used in this Letter. The continuous wave from the pump laser at 1950 nm is followed by a thulium-doped fiber amplifier, both manufactured by AdValue Photonics (Tucson, AZ). The residual ASE noise is suppressed by using a 1.55/1.95-μm wavelength division multiplexer (WDM_1). The atmosphere backscattering and the pump laser are combined and transferred into a PPLN-W via the second WDM_2. Optimized QPM condition is achieved by tuning the temperature of the PPLN-W with a thermoelectric cooler. Then backscattering photons at 1548 nm are converted into sum-frequency photons at 863 nm, which is collimated through an AR-coated objective lens and picked out by using a dichroic mirror. A volume Bragg grating (VBG) in conjunction with an 863-nm band pass filter (BPF) and a 945-nm short-pass filter (SPF) is used to block the second and higher order harmonics of the pump and the spontaneous Raman scattering. Finally, the 863-nm signal is focused onto a Si-APD (PicoQuant, τ-SPAD). The TTL signal corresponding to the photons received on the Si-APD is recorded on a multiscaler (FAST ComTec, MCS6A) and then processed in a computer. The optical layout of the upconversion detector is shown in Fig. 2. For the reader's convenience, key parameters of the micro-pulse aerosol lidar are listed in Table 1.

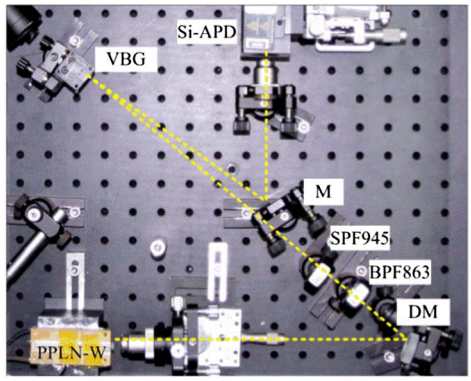

Fig. 2. Picture of the upconversion single-photon detector.

In addition to the advantages inherited from the detection laser at 1.5 μm, the micro-pulse lidar based on the upconversion detector has some other outstanding features for daytime operation. First, the waveguide only supports TM-polarized light, so the polarization states of the pump laser and the atmosphere backscattering should be aligned. This will suppress the sky radiance by a factor of 2. Second, the usage of VBG, BPF, and SPF in sequence results an ideal optical filter with background suppression >55 dB, bandwidth of 0.05 nm and transmission of 88%. Third, thanks to the quality of the Si: APD, a detection efficiency of 15% with the dark count noise of 40 Hz is realized at 1.5 μm, when the power of the 1950-nm pump laser is tuned to 25 mW, which allows integration of ultralow backscattering signal over a preset number of laser pulses.

Range-resolved recording of the backscattered signal allows the measurement of turbidity and, thus, of the

Table 1. Key Parameters of the Infrared Aerosol Lidar

Parameter	Value
Pulsed Laser	
Wavelength (nm)	1548.1
Pulse duration(ns)	300
Pulse energy (μJ)	110
Pulse repetition rate (kHz)	15
Pump Laser	
Wavelength (nm)	1950
Power (mW)	800
Collimator	
Aperture (mm)	100
Focal length (mm)	500
LMAF Mode-field diameter(μm)	20
Coupler	
Aperture (mm)	60
Focal length (mm)	150
SMF Mode-field diameter (μm)	10
PPLN waveguide	
QPM period (μm)	19.6
Length (mm)	52
Insert loss (dB)	1.5
Volume Bragg grating	
Reflection efficiency (%)	95
Bandwidth (nm)	0.05
Silicon APD	
Detection efficiency at 863 nm (%)	45
Dark count (Hz)	25

local visibility, which is not only significant to the public health but also important for all traffic operations and free-space optical communication. As a demonstration of the new micro-pulse lidar at 1.5 μm based on the up-conversion single-photon detector, the prototype system is operated horizontally for continuous measurement of atmospheric visibility.

As an example, experiment data over 24 h is shown in Fig. 3. The temporal resolution and spatial resolution are set to 300 s and 45 m, respectively. One can see from Fig. 3(a) that, even with only 110-μJ pulse energy and receiver diameter of 60 mm, the raw backscattering signal can extend to 7 km horizontally. During the experiment, smoke from the chimney of a power plant located 6.5 km away is detected four times from 20:00, Oct. 26, 2014 to 2:00, Oct. 27. One example of the smoke trace is shown in Fig. 3(b).

Note that Rayleigh scattering is inversely proportional to the fourth order of wavelength. Thus the main scattering source in the atmospheric backscattering is Mie scattering, and the photon number corresponding to the aerosol backscattering is described as

$$N(R) = E\eta_o \frac{\eta_q A_0}{h\nu R^2} \xi(R)\beta(R)\frac{c\tau_d}{2} \exp\left[-2\int_0^R \sigma(R)\mathrm{d}R\right], \quad (1)$$

where E is the energy of the laser pulse, and R is the range. η_0 accounts for the optical efficiency of the transmitted signal, η_q is the quantum efficiency, h is the Planck constant, A_0 is the area of the telescope, $\xi(R)$ is the geometrical overlap factor, $\beta(R)$ is the Mie volume backscattering coefficients, τ_d is the detector's response time, and $\sigma(R)$ is the atmospheric extinction coefficient. The geometrical overlap is calibrated in advance. By hypothesizing a constant ratio between $\sigma(R)$ and $\beta(R)$, an inversion algorithm proposed by Klett and Fernald is applied to retrieve $\sigma(R)$[1].

The relation between atmospheric visibility and the atmospheric attenuation coefficient is dependent on the physical characteristics of the hydrometeors as well as on the wavelength. According to a model [19], the relation is presented as

$$\sigma = \frac{3.91}{V}\left(\frac{\lambda}{550\ \mathrm{nm}}\right)^{-q}, \quad (2)$$

V is the atmospheric visibility in unit of km, λ is the detection wavelength in unit of nm, and q is the size distribution of the scattering particles, given by

$$q = \begin{cases} 1.6 & (V > 50\ \mathrm{km}) \\ 1.3 & (6\ \mathrm{km} < V < 50\ \mathrm{km}) \\ 0.16V + 0.34 & (1\ \mathrm{km} < V < 6\ \mathrm{km}) \\ V - 0.5 & (0.5\ \mathrm{km} < V < 1\ \mathrm{km}) \\ 0 & (V < 0.5\ \mathrm{km}) \end{cases}. \quad (3)$$

Finally, atmospheric visibility is retrieved according to Eq. (2), as shown in Fig. 4. The atmospheric humidity and temperature are recorded for reference.

The first peak of atmospheric attenuation coefficient occurs at the rush hour (18:00), which is due to the vehicle exhaust during the traffic congestion. The four bursts followed are due to the smoke in the sight of the optical antenna, as pointed out in Fig. 3. Between 2:00 and 8:00, the attenuation coefficient rises fast as the emergence of haze. After the sunrise, the attenuation coefficient

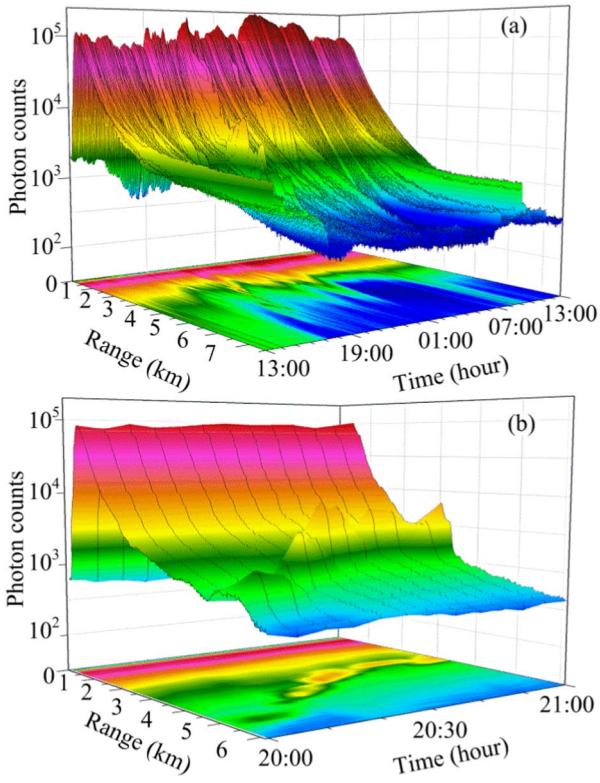

Fig. 3. Experiment raw data from lidar. (a) Backscattering signal of 24-hour continuous horizontal detection start at 13:00 on Oct. 26, 2014. (b) An example of smoke detected over one hour.

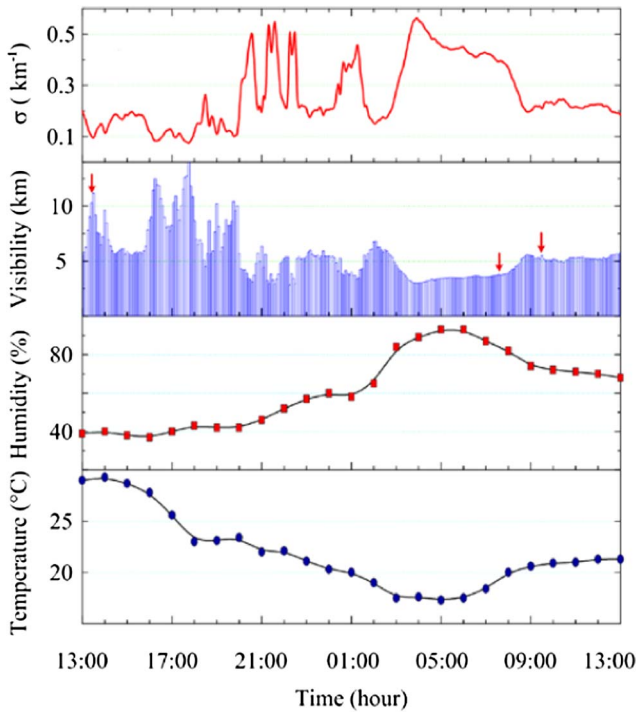

Fig. 4. Experiment results, from top to bottom, are extinction coefficient, visibility, humidity, and atmospheric temperature near ground.

Fig. 5. Photographs of the scene *in situ* under different weather conditions during the 24-hour lidar detection.

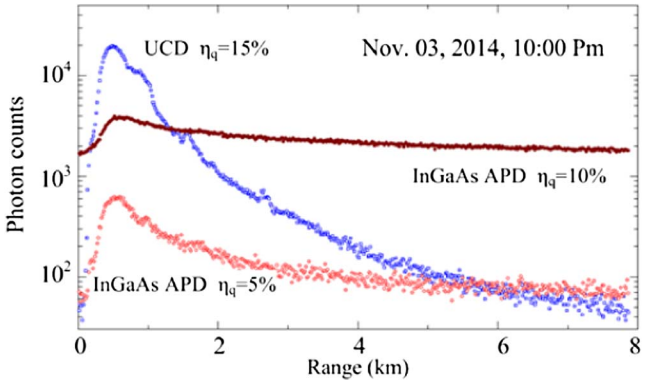

Fig. 6. Comparison between the InGaAs APD and the UCD.

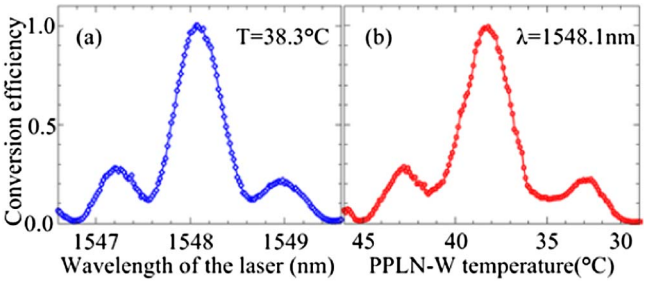

Fig. 7. (a) Conversion efficiency versus the frequency of the 1.5-μm seed laser. (b) Conversion efficiency versus the temperature of the PPLN-W.

declines as the drop/rise of the humidity/temperature. As shown in Fig. 5, the visibility values provided by the municipal meteorological bureau show good correspondence with the lidar detection.

After the visibility experiment, the UCD is compared to a commercial InGaAs APD (AUREA, APD-A), which operates in Geiger-mode at 20 MHz. The backscattering signals are plotted with an integral time of one minute, as shown in Fig. 6. Obviously, the signal-to-noise ratio using UCD is approximately two orders higher than that using the InGaAs APD. Although one can improve the quantum efficiency of the APD by raising its reverse voltage, the resulting dark counts will cover up the true aerosol backscattering.

In order to test the stability of our setup, the conversion efficiency is monitored using an optical spectrum analyzer (YOKOGAWA, AQ6370C) as shown in Fig. 7. A tunable laser is used to achieve the wavelength tuning curve of the PPLN-W at temperature of 38.3°C. The conversion efficiency is beyond 90% while the wavelength drift of the 1548.1-nm laser is less than 0.2 nm, as shown in Fig. 7(a). Then, a temperature-tuning curve is measured by scanning the temperature of waveguide, as shown in Fig. 7(b). The conversion efficiency can be kept above 90% while the temperature is controlled within 38.3 ± 0.8°C.

In conclusion, for the first time, a long-range micropulse aerosol lidar incorporating upconversion detector was demonstrated for continuous aerosol detection during day and night. In future work, a polarization maintaining and all-fiber upconversion detector will be developed to improve the polarization stability and compactness of the lidar.

This work has been supported by the NFRP (2011CB921300, 2013CB336800), the NNSF of China (41174131, 41274151), and the CAS.

References

1. C. Weitkamp, *Lidar Range-Resolved Optical Remote Sensing of the Atmosphere* (Springer, 2005).
2. ANSI Standard Z136.1, American National Standard for the Safe Use of Lasers (American National Standards Institute, Inc., 2007).
3. S. M. Spuler and S. D. Mayor, Proc. SPIE **6681**, 668102 (2007).
4. W. Shi, Q. Fang, X. Zhu, R. A. Norwood, and N. Peyghambarian, Appl. Opt. **53**, 6554 (2014).
5. S. D. Mayor and S. M. Spuler, Appl. Opt. **43**, 3915 (2004).
6. H. N. Forrister, D. W. Roberts, A. J. Mercer, and G. G. Gimmestad, Appl. Opt. **53**, D40 (2014).
7. A. Petrova-Mayor and V. Wulfmeyer, Appl. Opt. **47**, 1522 (2008).
8. R. H. Hadfield, Nat. Photonics **3**, 696 (2009).
9. N. Namekata, S. Sasamori, and S. Inoue, Opt. Express **14**, 10043 (2006).
10. Z. L. Yuan, B. E. Kardynal, A. W. Sharpe, and A. J. Shields, Appl. Phys. Lett. **91**, 041114 (2007).
11. F. Marsili, V. B. Verma, J. A. Stern, S. Harrington, A. E. Lita, T. Gerrits, I. Vayshenker, B. Baek, M. D. Shaw, R. P. Mirin, and S. W. Nam, Nat. Photonics **7**, 210 (2013).
12. G. Shentu, J. S. Pelc, X. Wang, Q. Sun, M. Zheng, M. M. Fejer, Q. Zhang, and J. Pan, Opt. Exp. **21**, 13986 (2013).
13. R. E. Warburton, A. McCarthy, A. M. Wallace, S. Hernandez-Marin, R. H. Hadfield, S. W. Nam, and G. S. Buller, Opt. Lett. **32**, 2266 (2007).
14. A. D. Bouteyre, G. Canat, M. Valla, B. Augere, C. Besson, D. Goular, L. Lombard, J.-P. Cariou, A. Durecu, D. Fleury, L. Bricteux, S. Brousmiche, S. Lugan, and B. Macq, IEEE J. Sel. Top. Quantum Electron. **15**, 441 (2009).
15. G. J. Yates, T. E. McDonald, Jr., D. E. Bliss, S. M. Cameron, F. J. Zutavern, and P. A. Zagarino, Proc. SPIE **4308**, 19 (2001).
16. S. A. Kingsley, S. Sriram, and P. E. Powers, Proc. SPIE **5791**, 262 (2005).
17. Y. Bai, J. Yu, N. P. Barnes, S. Chen, M. Petros, and H. R. Lee, Proc. SPIE **5653**, 43 (2005).
18. T. H. Wong, J. Yu, Y. Bai, and W. Johnson, in *Conference on Lasers Electro-Optics*, OSA Technical Digest (Optical Society of America, 2014), paper JTu4A-114
19. I. I. Kim, B. McArthur, and E. Korevaar, Proc. SPIE **4214**, 26 (2001).